JAERI-M
82-164

TIME- AND SPATIAL-BEHAVIOURS OF METAL IMPURITY DURING NEUTRAL-BEAM INJECTION ON THE JFT-2 TOKAMAK

November 1982

Satoshi KASAI, Toshio HIRAYAMA, Toshihiko YAMAUCHI, Tatsuo SUGIE, Shin YAMAMOTO, Masaki MAENO, Seio SENGOKU, Norio SUZUKI, Yukitoshi MIURA, Hisato KAWASHIMA and Hiroaki OGAWA

日本原子力研究所
Japan Atomic Energy Research Institute

JAERI-Mレポートは，日本原子力研究所が不定期に公刊している研究報告書です。
入手の問合わせは，日本原子力研究所技術情報部情報資料課（〒319-11茨城県那珂郡東海村）あて，お申しこしください。なお，このほかに財団法人原子力弘済会資料センター（〒319-11 茨城県那珂郡東海村日本原子力研究所内）で複写による実費頒布をおこなっております。

JAERI-M reports are issued irregularly.
Inquiries about availability of the reports should be addressed to Information Section, Division of Technical Information, Japan Atomic Energy Research Institute, Tokai-mura, Naka-gun, Ibaraki-ken 319-11, Japan.

編集兼発行　日本原子力研究所
印　　刷　㈱高野高速印刷

JAERI-M 82-164

Time- and Spatial-Behaviours of Metal Impurity during Neutral-Beam Injection on the JFT-2 Tokamak

Satoshi KASAI, Toshio HIRAYAMA[+], Toshihiko YAMAUCHI, Tatsuo SUGIE[+], Shin YAMAMOTO, Masaki MAENO, Seio SENGOKU, Norio SUZUKI, Yukitoshi MIURA, Hisato KAWASHIMA and Hiroaki OGAWA

Division of Thermonuclear Fusion Research,
Tokai Research Establishment, JAERI

(Received October 30, 1982)

The detailed time- and spatial-behaviours of emissions from iron impurities with the different ionic charge were obtained in the JFT-2 deutrium discharges with co- or counter-injections. In co-injection, the iron impurity is driven out from the central region of the plasma, and in counter-injection, they appear to accumulate and the plasma is not disrupted. These enhanced diffusion of the iron impurity can well be explained by the neutral-beam induced effect (direct beam-impurity interaction and toroidal rotation of the plasma), predicted by the neoclassical theory.

Keywords: Plasma, Torus, Impurity, Transport, JFT-2, Neutral Beam Injection, Iron, Diffusion

---

+ Division of Large Tokamak Developement, Tokai Research Establishment, JAERI.

JFT－2トカマクの中性粒子入射における金属不純物の時間的および空間的振舞

日本原子力研究所東海研究所核融合研究部
河西　敏・平山俊雄[+]・山内俊彦・杉江達夫[+]
山本　新・前野勝樹・仙石盛夫・鈴木紀夫
三浦幸俊・川島寿人・小川宏明

（1982年10月30日受理）

高速中性粒子入射をプラズマ電流と同方向（Co-入射）あるいは逆方向（C_{TR}-入射）に行ったJFT－2重水素放電において，鉄不純物からの放射の詳細な時間的および空間的振舞が得られた。Co入射の場合には，鉄不純物はプラズマ中心領域から排除される。一方，C_{TR}-入射の場合には，中心へと集中するように見える。これらの現象は，理論的に予想されている中性粒子ビームによって誘起される効果（ビームと不純物との直接的な相互作用とプラズマのトロイダル方向への回転）によって良く説明できる。

＋　大型トカマク開発部

Contents

1. Introduction 1
2. Experimental Arrangement and Characteristics of Discharges 2
3. Experimental Behaviours of Iron Impurities 4
3.1 Time- and Spatial-Variations in the Discharges with Sawtooth Oscillations 5
3.2 Time-Variations in the Counter-Injected Discharges without Sawtooth Oscillations 8
4. Discussion and Conclusions 10
Acknowledgements 13
References 13

目　　次

1. 序 1
2. 実験配置と放電特性 2
3. 鉄不純物の実験的振舞 4
3.1 鋸歯状波振動を持つ放電における時間および空間変化 5
3.2 鋸歯状波振動のない放電における時間変化 8
4. 議論および結果 10
謝　辞 13
文　献 13

1. Introduction

Impurity behaviours in Ohmic heating tokamak plasmas have been investigated experimentally and theoretically. Explanation of the behaviours needs anomalous flux driven by the pressure gradients across a magnetic surface in addition to a usual neoclassical flux [1-3].

Recently, high-power neutral beam or radio frequency have been supplied to get high-temperature and high-beta tokamak plasmas. It has been pointed out experimentally and theoretically that radial transport of impurities and spectral-line emission from impurities are modified during auxiliary heating. Stacy and Sigmer [4], and Burrell et al. [5] suggested that neutral-beam injection parallel to the plasma current (co-injection) expels impurities, whereas counter-injection drives them in due to direct beam-impurity interaction and plasma rotation in the toroidal direction within the framework of neoclassical transport theory. But some theorists have obtained a different prediction, i.e. co-injection induces inward diffusion and counter-injection is reverse [6-8].

The ISX-B and PLT experiments have shown dramatic changes in the impurity content and radial profiles (PLT experiments) during neutral-beam injection [9,10]. Isler [9] examined the beam effect on the discharge with sawtooth oscillation (a very low level of MHD activity and concluded that neoclassical beam-induced effects seem to increase the accumulation rates of impurities during counter-injection, but the co-injection results are not clear for the beam effect. Burrell [5] explained the experimental results in co- and counter-injections in the ISX-B and PLT tokamaks by the effect of plasma rotation.

The another beam effect on impurity behaviour is charge transfer between fast- and halo-neutrals due to beam injection and highly-ionized

impurity ions. This atomic process enhances spectral-line emission from impurity ions and modify the population density of impurity ions in each charge state [11]. Thus, this is very important on the estimation of the impurity diffusion coefficient.

In the ISX-B [12] and DITE [13] discharges with low density (n_e= $(2\sim3)\times10^{13}$ cm^{-3}), observed enhancements of spectral-line emission from light and metal impurity ions (rise time≈1∿2 ms) were explained by charge transfer, espetially, spatial distribution of impurities in DITE is much better described by the numerical code including charge-exchange recombination than without it.

In the JFT-2 tokamak, the time- and spatial-behaviours of emissions from Fe^{9+}, Fe^{14+}, Fe^{17+}, and Fe^{18+} ions were measured in the neutral-beam injected discharges with and without sawtooth oscillations.

In the next section, we describe the experimental arrangement and the characteristics of the discharges. The time- and spatial-behaviours of iron impurities are shown in the section 3. In the last section, we discuss the charge transfer between the fast- and halo-neutrals and iron impurities, and the neoclassical beam effect on the iron impurity behaviours.

2. Experimental Arrangement and Characteristics of Discharges

A schematic view of the JFT-2 tokamak and the principal diagnostic equipments are shown in Fig.1. The directions of the plasma current and the toroidal field are clockwise and counter-clockwise, respectivelly. The neutral beam injectors are placed at 40 degrees with the minor axis of the torus. Maximum injected power of the each beam line is about 1 MW at 40 kV and 32 A. The beam pulse duration is about 100 ms. The rise-time of the beam is about 100 μs. The rail-limiter, placed at the top of the

impurity ions. This atomic process enhances spectral-line emission from impurity ions and modify the population density of impurity ions in each charge state [11]. Thus, this is very important on the estimation of the impurity diffusion coefficient.

In the ISX-B [12] and DITE [13] discharges with low density (n_e= (2∿3)×10^{13} cm^{-3}), observed enhancements of spectral-line emission from light and metal impurity ions (rise time≃1∿2 ms) were explained by charge transfer, espetially, spatial distribution of impurities in DITE is much better described by the numerical code including charge-exchange recombination than without it.

In the JFT-2 tokamak, the time- and spatial-behaviours of emissions from Fe^{9+}, Fe^{14+}, Fe^{17+}, and Fe^{18+} ions were measured in the neutral-beam injected discharges with and without sawtooth oscillations.

In the next section, we describe the experimental arrangement and the characteristics of the discharges. The time- and spatial-behaviours of iron impurities are shown in the section 3. In the last section, we discuss the charge transfer between the fast- and halo-neutrals and iron impurities, and the neoclassical beam effect on the iron impurity behaviours.

2. Experimental Arrangement and Characteristics of Discharges

A schematic view of the JFT-2 tokamak and the principal diagnostic equipments are shown in Fig.1. The directions of the plasma current and the toroidal field are clockwise and counter-clockwise, respectivelly. The neutral beam injectors are placed at 40 degrees with the minor axis of the torus. Maximum injected power of the each beam line is about 1 MW at 40 kV and 32 A. The beam pulse duration is about 100 ms. The rise-time of the beam is about 100 μs. The rail-limiter, placed at the top of the

4th port, and the vacuum vessel are stainless-steel. In order to reduce light impurities, titanium is gettered on the torus wall before the discharge and in the interval of discharges.

The line-integrated emission from light and metal impurities were measured by using the 3m grazing-incidence monochromator, and the spatial distribution of the emissions (spectral-line emissions from impurities integrated along the line of sight) were obtained by tilting the monochromator. The time- and spatial-variations of the electron temperature and density were measured by the Thomson scattering apparatus. The central ion temperature and its radial profile were obtained from the energy-spectrum analysis of charge-exchanged neutrals and measurements of Doppler profiles of impurity ions ionized in the different charge-states (e.g. TiXVIII, TiXIV, OVII, and CV). The 2mm and 4mm μ-wave interferometers were used to get the line-averaged electron density. The soft X-ray radiation from the central region of the plasma and the horizontal shift of the hot plasma column were measured by the pin-diode array equipted horizontally and vertically.

Characteristics of the typical discharges with neutral-beam injection (beam power P_b=1 MW (38 kV, 65 A)) in the study of the impurity behaviour are shown in Fig.2. The strength of the toroidal field B_t is 13 kG and the plasma current I_p increases to about 130 kA during the Ohmic heating phase and gradually increases during the injection phase. The energetic hydrogen beam (H^0) is injected at 100 ms to a deutrium asma (D^+) with the minor radius of 25 cm in the co- and counter-directions. During injection, the one-turn loop voltage decreases to about 1.2 (solid-line) and 1.5 volts (dotted-line) in the co- and counter-injection phases (no correction for the change of the plasma inductance), respectively.

The line-averaged electron density increases linearly, which is kept by puffing additional gas during injection. The central electron temperature $T_e(0)$ increases from about 440 eV at 100 ms to 800∿900 eV during co-injection, and to 630 eV during counter-injection. The central ion temperature is 650∿750 eV at 120 ms and 500∿600 eV at 115 ms in co- and counter-injections, respectively. The spatial distribution of the ion temperature is determined from the width of the Doppler broadening of the TiXIV (λ=2117 Å), OVII (λ=1623 Å) and CV (λ=2271 Å) lines. The plasma boundary temperature obtained from an electrostatic probe measurement is 25∿30 eV from 105 ms to 125 ms and increases linearly to 40 eV at 130 ms during co-injection. On the other hand, this temperature increases monotonously from 25 eV (at 100 ms) to 50 eV (at 130 ms) in counter-injection.

In the above-mentioned discharges, the sawtooth oscillations are dominant during the discharge as shown in Fig.3. The amplitude of sawtooth signals during injection is larger than that in the Ohmic heating phase, especially, the amplitude after about 120 ms in counter-injection is very large. The soft X-ray intensity increases up to 120 ms and saturates in both discharges.

The characteristics of the another discharges without sawtooth oscillations, but with high frequency of about 10 kHz during injection are similar to the above-mentioned discharges, except that the plasma current is low by 12∿15 % and the line-averaged electron density is high by 6∿23 %.

3. Experimental Behaviours of Iron Impurities

Line-integrated emissions from iron ions (Fe^{9+}, Fe^{14+}, Fe^{17+}, Fe^{18+}) were observed by using the absolutely-calibrated grazing-incidence

The line-averaged electron density increases linearly, which is kept by puffing additional gas during injection. The central electron temperature $T_e(0)$ increases from about 440 eV at 100 ms to 800∿900 eV during co-injection, and to 630 eV during counter-injection. The central ion temperature is 650∿750 eV at 120 ms and 500∿600 eV at 115 ms in co- and counter-injections, respectively. The spatial distribution of the ion temperature is determined from the width of the Doppler broadening of the TiXIV (λ=2117 Å), OVII (λ=1623 Å) and CV (λ=2271 Å) lines. The plasma boundary temperature obtained from an electrostatic probe measurement is 25∿30 eV from 105 ms to 125 ms and increases linearly to 40 eV at 130 ms during co-injection. On the other hand, this temperature increases monotonously from 25 eV (at 100 ms) to 50 eV (at 130 ms) in counter-injection.

In the above-mentioned discharges, the sawtooth oscillations are dominant during the discharge as shown in Fig.3. The amplitude of sawtooth signals during injection is larger than that in the Ohmic heating phase, especially, the amplitude after about 120 ms in counter-injection is very large. The soft X-ray intensity increases up to 120 ms and saturates in both discharges.

The characteristics of the another discharges without sawtooth oscillations, but with high frequency of about 10 kHz during injection are similar to the above-mentioned discharges, except that the plasma current is low by 12∿15 % and the line-averaged electron density is high by 6∿23 %.

3. Experimental Behaviours of Iron Impurities

Line-integrated emissions from iron ions (Fe^{9+}, Fe^{14+}, Fe^{17+}, Fe^{18+}) were observed by using the absolutely-calibrated grazing-incidence

monochromator in co- and counter-injected discharges with and without sawtooth oscillations.

3.1 Time- and Spatial-Variations in the Discharges with Sawtooth Oscillations

Figure 4 shows the time-evolutions of the radiance of FeXVIII (λ= 93.9 Å), FeXV (λ=284.2 Å) and FeX (λ=174.5 Å) lines measured along the chords at the vertical positions (Z=0, -10, -12, -14, -16 cm) on the lower-half of the torus in co- and counter-injections. Gradual increases of the emissions from Fe^{9+} ions in the Ohmic heating phase and during neutral-beam injection are due to the influx of the iron impurity, because that the increasing rate of the electron density is slower than that of the emission and the radiance should decrease when the electron temperature increases. The small decrease of the FeXV emission, for about 5 ms after injection is due to ionization to upper states by increment of the electron temperature. The radiance of the FeXVIII line changes from 2.5×10^{14} photons.cm^{-2}.sec^{-1} (100 ms) to 6×10^{14} photons.cm^{-2}.sec^{-1} (115 ms) and indicates very slow increase or saturation in co-injection. On the other hand, in counter-injection, the radiance exponentially goes up to ten-times that at 100 ms untill about 120 ms, but suddenly the increase stops and radiance gradually decrease [14].

In both cases, the time-evolutions of the spatial distributions of the radiation (FeXVIII line) integrated along the line of sight versus the vertical position Z on the lower-half of the torus are shown in Fig.5. Before injection (Ohmic heating phase), the distributions and the amount of the radiation are similar to each other. During injection in the co-direction, as shown in Fig.5a, the profiles become shallow-hollow. On the other hand, in counter-injection, the distributions become peaked profile with time. The former profiles are slightly broad in comparison to those

in the latter case.

Above-mentioned tendency can also be seen in Fig.6. The radiation powers of FeXVIII line from the central regime ($r \leq 5$ cm, r : minor radius of the plasma) and the regime of $0 \leq r \leq 10$ cm are indicated in co- and counter-injections. The radiation power in the central region in counter-injection (open triangle) is twice that in co-injection (open circle) from 117 ms to 130 ms, but the power level saturates at about 1.0 kW and 0.5 kW, respectively. In the region of $0 \leq r \leq 10$ cm, the discrepancy of the power (comparison between dashed and dotted curves) is only 40∿28 % in the same time interval. This fact indicates that the radial distribution of radiation in counter-injection is peaked and concentrates near the plasma center, and in co-injection, there may be the enhanced reduction of the impurity in the central region. In the initial phase during injection, the increasing rate of the radiation in counter-injection is larger than that in co-injection in both regimes.

On co-injection, the time behaviours (i.e. the tendency of the saturation of FeXVIII line radiation) as shown in Figs.4 and 6 are very similar to those in the ISX-B tokamak [9].

On counter-injected discharges after about 120 ms, the increase of the radiation stops suddenly and saturates, and the plasma is not disrupted during injection. This phenomenon seems to correlate with the appearance of sawtooth oscillations with the large amplitude, although the oscillation appears slightly faster than the stop of the radiation increase as shown in Fig.3. In this phase of the discharge, large impurity loss appears to exist in the central regime of the plasma (the electron density indicates a gradual increase and the central electron temperature is nearly constant), although we have not any data indicated directly the loss of impurity ions, e.g. particle confinement

time of impurity ions. However, the saturation of influx of iron may reflect to this phenomenon. The fast decrement after 130 ms is mainly due to the decrease of the central electron temperature by the excess radiation cooling.

The radiation power depends directly and indirectly on the electron density and temperature. Thus, we also made comparison of the population density of the Fe^{17+} ion in between co- and counter-injections. Figure 7 shows the Abel-inverted spatial distributions of the density of Fe^{17+}, Fe^{14+}, and Fe^{9+} ions in the ground state at 100 (start point of neutral-beam injection), 115, 120 and 130 ms. In these evaluations, the experimentally obtained time- and radial-variations of the electron temperature and density are used except the profiles at 115 and 120 ms in counter-injection (at these points they are assumed to be the same profile with that at 130 ms).

In co-injection, the population density of Fe^{17+} ion indicates a gradual increase with time (a factor of 1.7), and its profile is shallow-hollow during injection. The profile of Fe^{9+} ion becomes broad after injection, but the density at the peak changes slightly. The total number of this ion only indicates the increase of 33∿37 %. In counter-injection, the population density of Fe^{17+} ion near the plasma center ($r \leq 5$ cm) at 120 ms increases to about 6 times that at 100 ms, although there are uncertainty of the Abel-inversion near the plasma center and the assumed profiles of the electron density and temperature. From 120 to 135 ms, the density is approximately constant. The time-variation of Fe^{9+} ion is similar to that in co-injection (the increasing rate of the total number of this ion is about 40 %).

There should exist Fe^{18+} and Fe^{16+} ions under these discharge conditions, but we did not measure. Thus, we roughly estimated by using

the coronal equilibrium equation (particle confinement time is larger than the characteristic time of electron collision ionization). The density of the Fe^{18+} ion near the plasma center is 1.4 times (co-injection) and 1.7 times (counter-injection) those of Fe^{17+} ion at 130 ms, respectively. The density of Fe^{16+} ion is about 0.7 times that of Fe^{17+} ion in both cases.

Above-mentioned experimental results indicate that, in counter-injection, there is accumulation of the iron impurity into the central region of the plasma. This accumulation appeares to be enhanced by the increase of the influx and/or by the neoclassical beam effect [4,5]. The cause of the accumulation is not yet clear in this case. In co-injection, the iron impurities may be driven out from the central region of the plasma, because the content of iron density saturates in spite of the increase of the influx, and the radiance of the FeXVIII line near the central region should increase when the electron temperature increases. This drive-out may be due to the neoclassical beam effect if the anomalous diffusion, which is usual diffusion in the Ohmic heating phase, does not change during injection. After about 120 ms, the accumulation appears to be relaxed with slight time-delay. This relaxation seems to correlate with the large amplitude sawtooth oscillation or may be due to the saturation of influx of iron.

3.2 Time-Variations in the Counter-Injected Discharges without Sawtooth Oscillations

The discharge condition is very similar to that in subsection 3.1, as described in section 2. There is no sawtooth oscillation, but oscillation with high frequency of about 10 kHz during injection.

Figure 8a shows the time-variations of the radiance of FeX, FeXV, FeXVIII and FeXIX (λ=108.4 Å) lines measured along the central chord (Z=

0). In order to comparison, the time-behaviours of the radiance of the same iron spectral-lines in the co-injected discharge with sawteeth, not including a large amplitude sawtooth oscillation as in subsection 3.1, are shown in Fig.8b. In both cases, when the neutral beam injects, the emissions from ions in low-ionized states (Fe^{9+} and Fe^{14+}) decrease by raise of the electron temperature, and the behaviours of the radiance of the FeX line indicate that the iron influx does not increase.

In the early phase of counter-injection, the radiances of the FeXVIII and FeXIX lines are about one order greater than those before injection, but after 120 ms they diminish fast (corresponding to this decrease, the radiances of FeX and FeXV lines increase through recombination process). This is due to the excess radiation cooling near the central region of the plasma.

Figure 9 shows the time-evolutions of the line-averaged population density of Fe^{17+} and Fe^{18+} ions in the ground state during counter-injection (the co-injected case also indicates). These estimations are rough, because, in these cases, the spatial distributions of radiances from iron ions and the profiles of the electron density and temperature are not obtained. This figure shows that the population density increases with time untill about 120 ms and decreases.

From the results in Figs.8 and 9, it is found that the excess radiation cooling results from the accumulation of the iron impurity near the central region of the plasma. In this case, this accumulation can not be explained by the iron influx, because the influx does not increase during counter-injection. Thus, the neutral beam injected in the counter-direction acts to accumulate impurities into the central region of the plasma. However, the degree of the effect seems to be different in both counter-injections in subsections 3.1 and 3.2, that is, there

may be another effect influenced delicately on the accumulation.

4. Discussion and Conclusions

In a few tokamak plasma with neutral-beam injection, the observed enhancement of the emission from impurity ions is explained by charge transfer between fast- and halo-neutrals by injection and impurity ions [10-13]. Thus, this process can not always be neglected on the impurity behaviour. The characteristics of the effect by this process on spectral emissions are the fast rise (1∿2 ms), except PLT results, and to be observed in the relatively low electron density ($\bar{n}_e \leq 2\sim3\times10^{13}$ cm^{-3}).

In our cases, the grazing-incidence monochromator used measurements of line-integrated spectral emissions is placed to view the field including high-energy hydrogen atoms from co-injected beam, but not atoms from counter-injected beam.

The transit time of ions in the torus direction is an order of 10^{-5} sec. The characteristic time for electron collision ionization is $(0.5\sim3)\times10^{-3}$ sec for Fe^{18+}, Fe^{17+}, O^{7+} ions. The life-time of the pertinent excited states is about 10^{-11} sec. The electron collision excitation time is less than 1 ms for Fe^{18+} and Fe^{17+} ions and several ms for O^{7+} ion. On the time-history of emissions of the iron spectral-lines, the enhanced emission with fast rise should be observed in both co- (contribution of fast-and halo-neutrals) and counter- (halo-neutrals) injected discharges. The enhancement were not observed even in co-injection. It is thought to be due to attenuation of the fast atoms of the beam by electron collision before they reach the view point because of high density ($\bar{n}_e \geq (4\sim5)\times10^{13}$ cm^{-3}) during injection.

The results of the numerical calculations for charge transfer between fast- and halo-neutrals and iron ions indicate that this atomic

may be another effect influenced delicately on the accumulation.

4. Discussion and Conclusions

In a few tokamak plasma with neutral-beam injection, the observed enhancement of the emission from impurity ions is explained by charge transfer between fast- and halo-neutrals by injection and impurity ions [10-13]. Thus, this process can not always be neglected on the impurity behaviour. The characteristics of the effect by this process on spectral emissions are the fast rise (1∿2 ms), except PLT results, and to be observed in the relatively low electron density ($\bar{n}_e \leq 2\sim3\times10^{13}$ cm^{-3}).

In our cases, the grazing-incidence monochromator used measurements of line-integrated spectral emissions is placed to view the field including high-energy hydrogen atoms from co-injected beam, but not atoms from counter-injected beam.

The transit time of ions in the torus direction is an order of 10^{-5} sec. The characteristic time for electron collision ionization is $(0.5\sim3)\times10^{-3}$ sec for Fe^{18+}, Fe^{17+}, O^{7+} ions. The life-time of the pertinent excited states is about 10^{-11} sec. The electron collision excitation time is less than 1 ms for Fe^{18+} and Fe^{17+} ions and several ms for O^{7+} ion. On the time-history of emissions of the iron spectral-lines, the enhanced emission with fast rise should be observed in both co- (contribution of fast-and halo-neutrals) and counter- (halo-neutrals) injected discharges. The enhancement were not observed even in co-injection. It is thought to be due to attenuation of the fast atoms of the beam by electron collision before they reach the view point because of high density ($\bar{n}_e \geq (4\sim5)\times10^{13}$ cm^{-3}) during injection.

The results of the numerical calculations for charge transfer between fast- and halo-neutrals and iron ions indicate that this atomic

process influences slightly on the spectral-line emission from iron ions, because the ionization process is dominant and the content of Fe^{19+} and Fe^{20+} ions is small (content of these ions decreases by 20∿30 % through the charge transfer process).

In order to investigate the transport of iron ions, we used the numerical calculations, considering the electron collision ionization, radiative and dielectronic recombinations, charge transfer between fast- and halo-neutrals and iron ions, neoclassical diffusion in the Pfirsch-Schlüter regime by Samain and Werkoff, and anomalous diffusion by density gradient of impurity ions, but not including the neutral-beam effect, i.e. enhancement of radially outward or inward diffusion flux driven by the direct momentum input to the plasma particles and the toroidal rotation of the plasma induced by beam injection. Both radial- and time-behaviours could not reasonably be explained by this numerical transport model of impurity, even though the profiles and values of the electron temperature and density are changed within the experimental error. It is found that the increase of the iron influx also increases the radiation of the FeXVIII line with time and the discrepancy from the experimental results becomes larger. The radial profiles are not influenced by the influx, i.e. they are mainly determined by the profiles of the electron temperature and density and diffusion coefficients. Thus, the behaviours can not be explained by the difference of the influx ($1\times10^{17}\sim9\times10^{17}$ sec^{-1}), especially for co-injection. Also, the difference of anomalous diffusion coefficients (D_a=4000 cm^2/s or $1\times10^{17}/n_e$ (Alcator scaling)) is the minor effect on the time- and spatial-variations (less than 16 % for FeXVIII and FeXV line radiances and about 26 % for FeX line radiance).

On the recent numerical calculations including the beam effect, the time- and radial-behaviours of Fe^{17+}, Fe^{14+} and Fe^{9+} ions can be

explained by considering the enhanced outward diffusion with the velocity of about 10 m/s, which is assumed to be due to the neoclassical beam effect (direct momentum input and toroidal plasma rotation), and the influx of 5×10^{17} s^{-1} in co-injection. For counter-injection, assuming the inward velocity of 5∿10 m/s, the experimental behaviours can be explained, except the time-behaviours of FeXV line radiance. There may still be some unknown factors on the counter-injected discharges.

From present experimental and numerical results, we conclude that iron impurities drive out from the central region of the plasma by co-injection, and they appears to accumulate into the center by counter-injection, but the plasma is not disrupted during counter-injection.

Acknowledgements

The authors are very grateful to Drs. T. Matoba and T. Shoji and other members of the experimental plasma physics laboratory for their helpful discussions and co-operation, and Messrs. Y. Matsuzaki, K. Anno and T. Shibata and their crew for operation of the JFT-2 device and the neutral-beam injectors. The authors would like to Drs. A. Funahashi, Y. Tanaka, M. Tanaka and Y. Obata for their continuous encouragement to the present work.

References

1) T.F.R. Group : Plasma Phys. 20 (1978) 735.

2) R.J. Hawryluk, S. Suckewer, S.P. Hirshman : Nucl. Fusion 19 (1979) 607.

3) T.F.R. Group : EUR-CEA-FC-1146 (March 1982), "Light Impurity Transport in the TFR Tokamak Comparison of Oxygen and Carbon Line Emission with Numerical Simulations".

4) W.M. Stacey, Jr., D.J. Sigmar : Nucl. Fusion 19 (1979) 1665, Phys. Fluids 22 (1979) 2000.

5) K.H. Burrell, T. Ohkawa, S.K. Wong : Phys. Rev. Letters 17 (1981) 511.

6) T. Ohkawa : Kaku Yugo Kenkyu 32 (1974) 1.

7) Z.El-Derini, G.A. Emmert : Nucl. Fusion 16 (1976) 342.

8) P.B. Parks, K.H. Burrell, S.K. Wong : Nucl. Fusion 20 (1980) 27.

9) R.C. Isler, L.E. Murray, S. Kasai, D.E. Arnurius, S.C. Bates, et al. : Phys. Rev. Letters 31 (1981) 649.

10) S. Suckewer, E. Hinnov, D. Hwang, J. Schivell, G.L. Schmidt et al. :

Acknowledgements

The authors are very grateful to Drs. T. Matoba and T. Shoji and other members of the experimental plasma physics laboratory for their helpful discussions and co-operation, and Messrs. Y. Matsuzaki, K. Anno and T. Shibata and their crew for operation of the JFT-2 device and the neutral-beam injectors. The authors would like to Drs. A. Funahashi, Y. Tanaka, M. Tanaka and Y. Obata for their continuous encouragement to the present work.

References

1) T.F.R. Group : Plasma Phys. 20 (1978) 735.

2) R.J. Hawryluk, S. Suckewer, S.P. Hirshman : Nucl. Fusion 19 (1979) 607.

3) T.F.R. Group : EUR-CEA-FC-1146 (March 1982), "Light Impurity Transport in the TFR Tokamak Comparison of Oxygen and Carbon Line Emission with Numerical Simulations".

4) W.M. Stacey, Jr., D.J. Sigmar : Nucl. Fusion 19 (1979) 1665, Phys. Fluids 22 (1979) 2000.

5) K.H. Burrell, T. Ohkawa, S.K. Wong : Phys. Rev. Letters 17 (1981) 511.

6) T. Ohkawa : Kaku Yugo Kenkyu 32 (1974) 1.

7) Z.El-Derini, G.A. Emmert : Nucl. Fusion 16 (1976) 342.

8) P.B. Parks, K.H. Burrell, S.K. Wong : Nucl. Fusion 20 (1980) 27.

9) R.C. Isler, L.E. Murray, S. Kasai, D.E. Arnurius, S.C. Bates, et al. : Phys. Rev. Letters 31 (1981) 649.

10) S. Suckewer, E. Hinnov, D. Hwang, J. Schivell, G.L. Schmidt et al. :

Nucl. Fusion 21 (1981) 981.

11) S. Suckewer, E. Hinnov, M. Bitter, R. Hulse, D. Post : Phys. Rev. 22A (1980) 725.

12) R.C. Isler, L.E. Murray, S. Kasai, J.L. Dunlap, S.C. Bates, P.H. Edmonds, et al. : Phys. Rev. 24A (1981) 2701.

13) W.H.M. Clark, J.G. Cordey, M. Cox, S.J. Fielding, R.D. Gill, et al. : Nucl. Fusion 22 (1982) 333.

14) S.Yamamoto, M. Maeno, S. Sengoku, N. Suzuki, S. Kasai, et al. : 9th Int. Conf. on Plasma Physics and Controlled Nuclear Fusion Research (Baltimore) 1982, IAEA-CN-41/A-5.

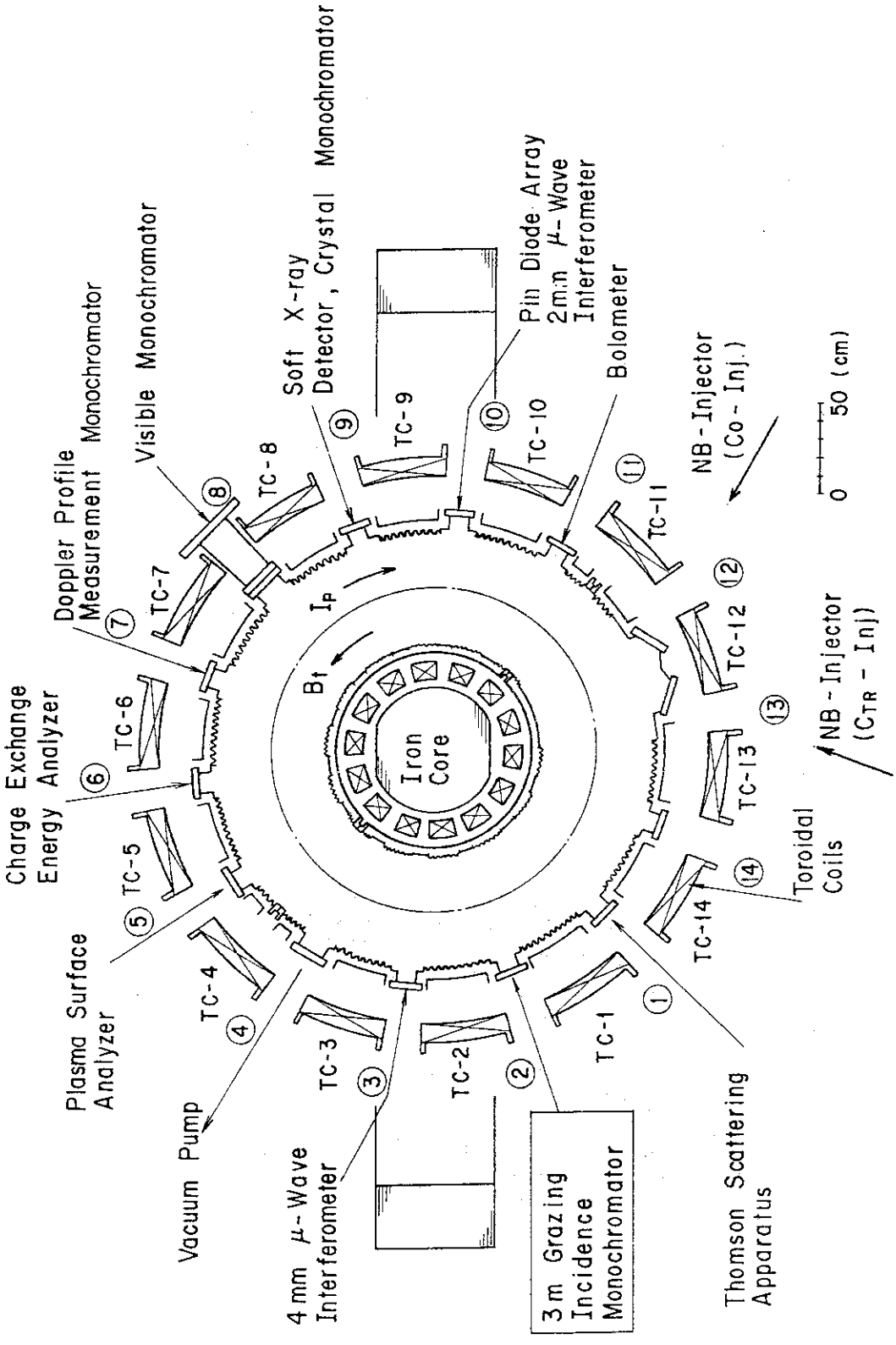

Fig. 1 The schematic view of the JFT-2 tokamak with neutral-beam injectors and the principal diagnostic equipments.

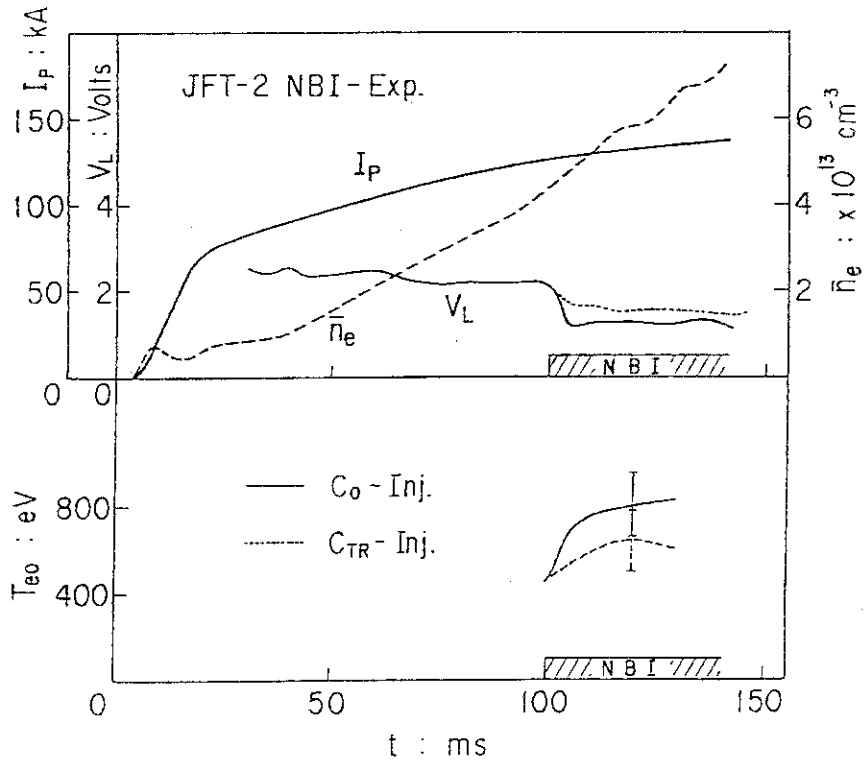

Fig. 2 Characteristics of a typical discharge with neutral-beam injection, toroidal field B_t=13 kG, I_p: plasma current, V_1: one-turn loop voltage, $\bar{n}_e$: line-averaged electron density, $T_e(0)$: central electron temperature.

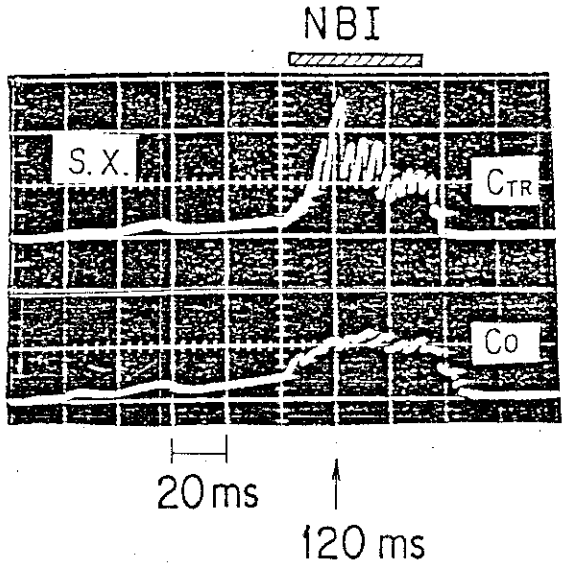

Fig. 3 Signals of sawtooth oscillation measured by pin-diode array in the Ohmic and beam heating phases; upper trace: counter-injection, lower trace: co-injection.

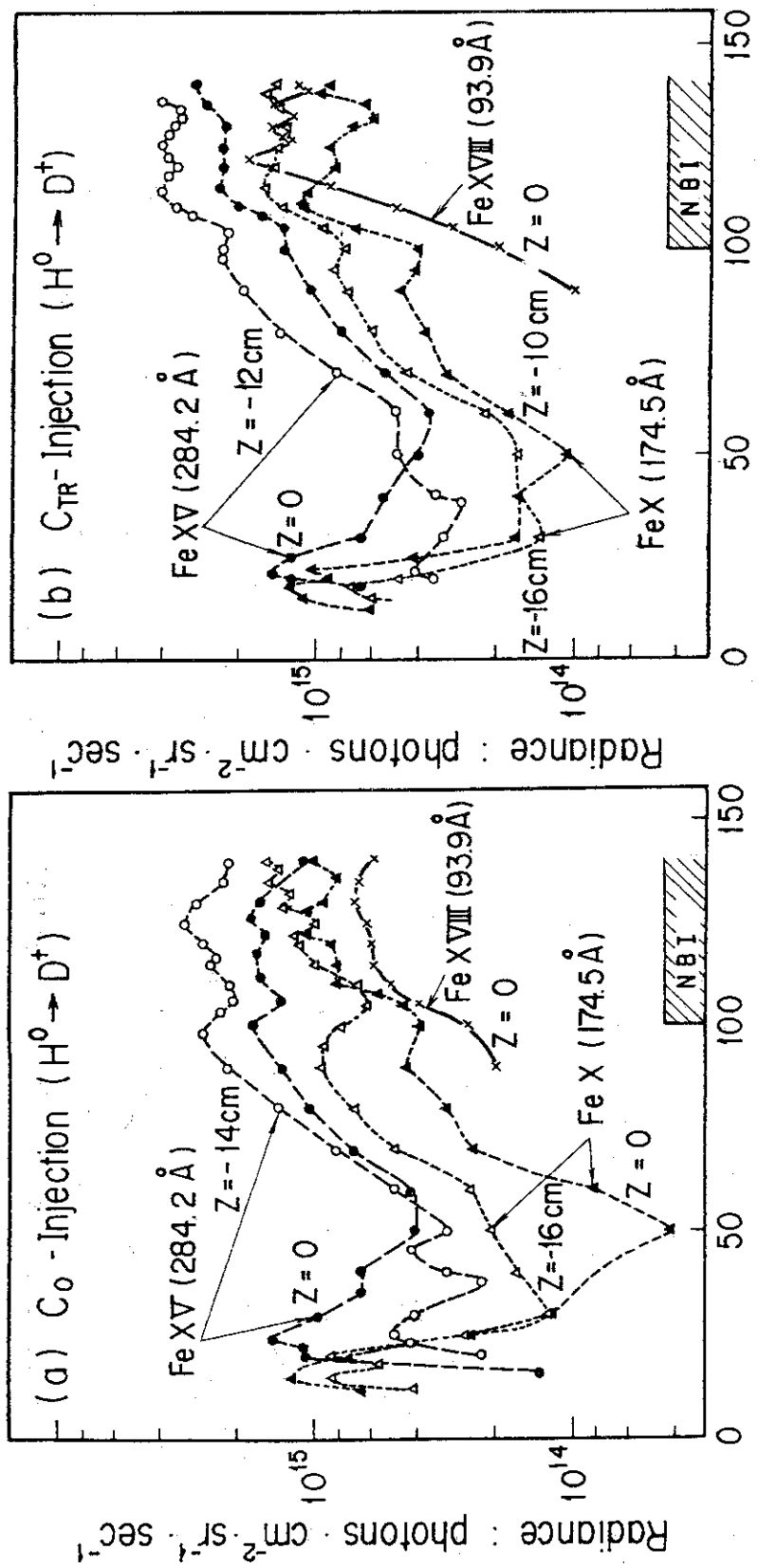

Fig. 4 Time-evolutions of the radiance of FeXVIII (λ=93.9 Å), FeXV (λ=284.2 Å) and FeX (λ=174.5 Å) lines measured along the chord of Z=0, -10, -12, -14, -16 cm in co- and counter-injections.

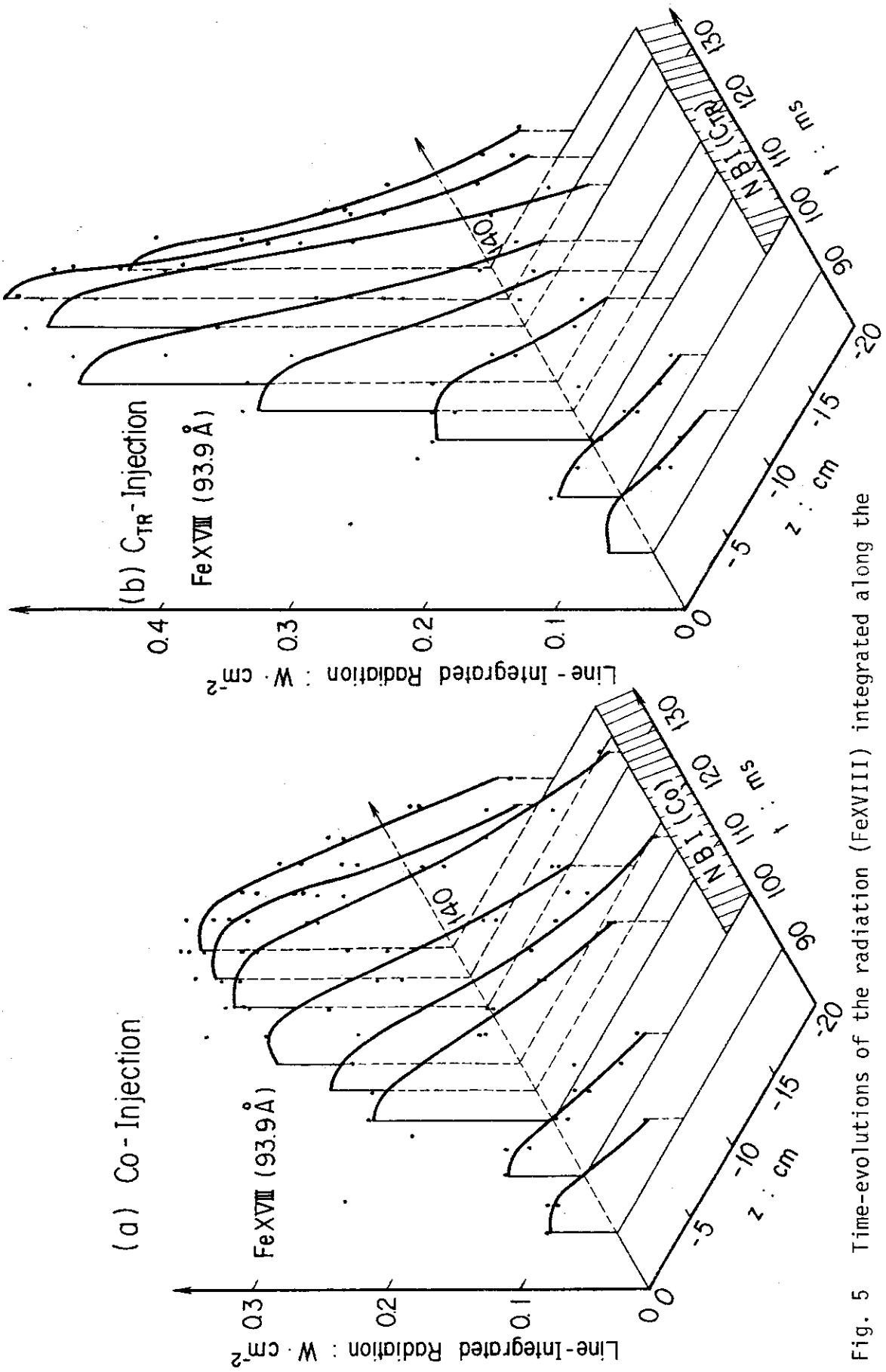

Fig. 5 Time-evolutions of the radiation (FeXVIII) integrated along the line of sight on the lower-half of the torus in co-injection (a) and counter-injection (b).

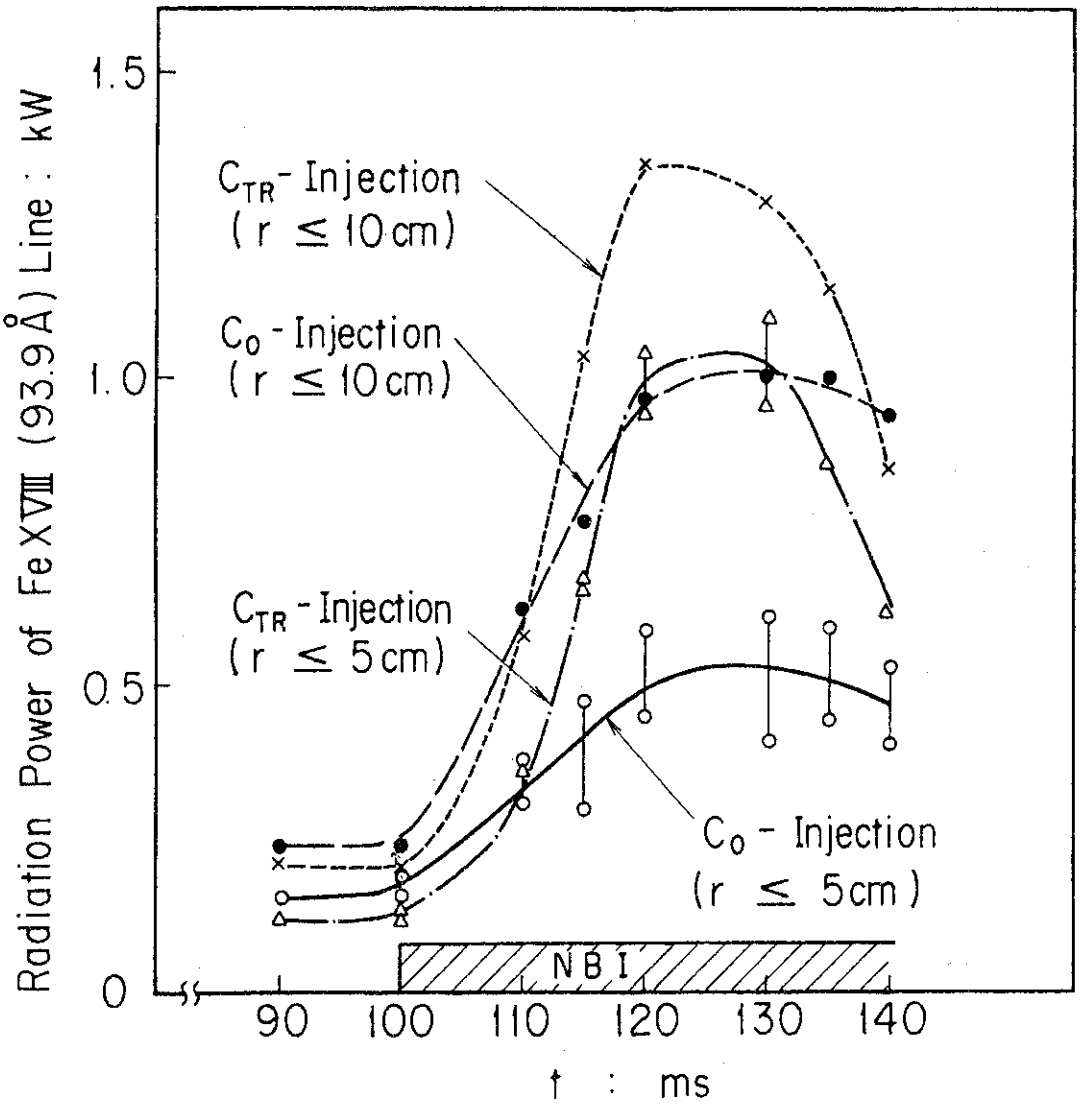

Fig. 6 Time-variations of radiation power of FeXVIII (λ=93.9 Å) in the central regime of the plasma ($r \leq 5$ cm) and the regime of $0 \leq r \leq 10$ cm in co- (open and closed circles) and counter- (open triangle and cross) injections.

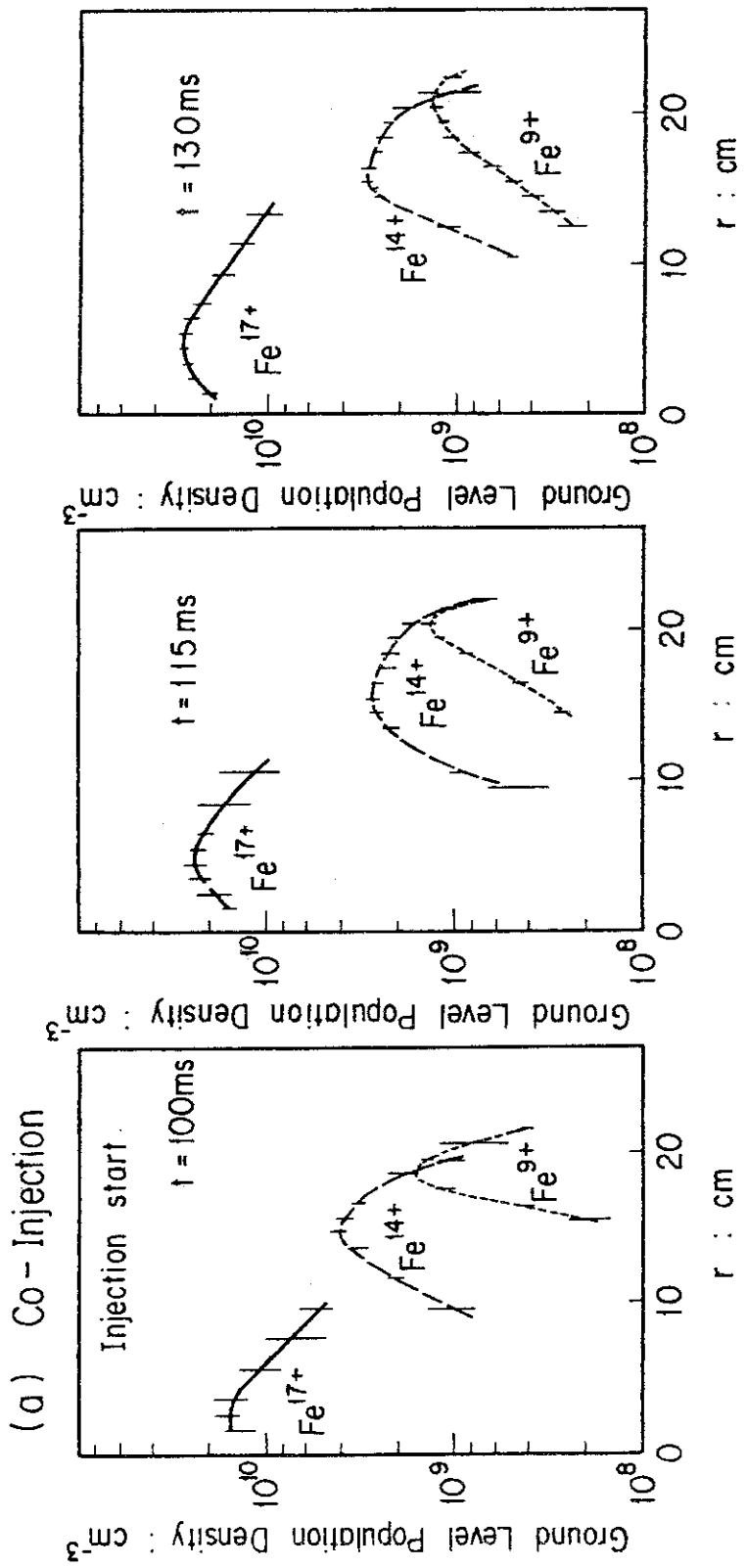

Fig. 7(a) Radial distributions of the population density of the Fe^{17+}, Fe^{14+} Fe^{9+} ions in the ground state in co- (a) and counter- (b) injections.

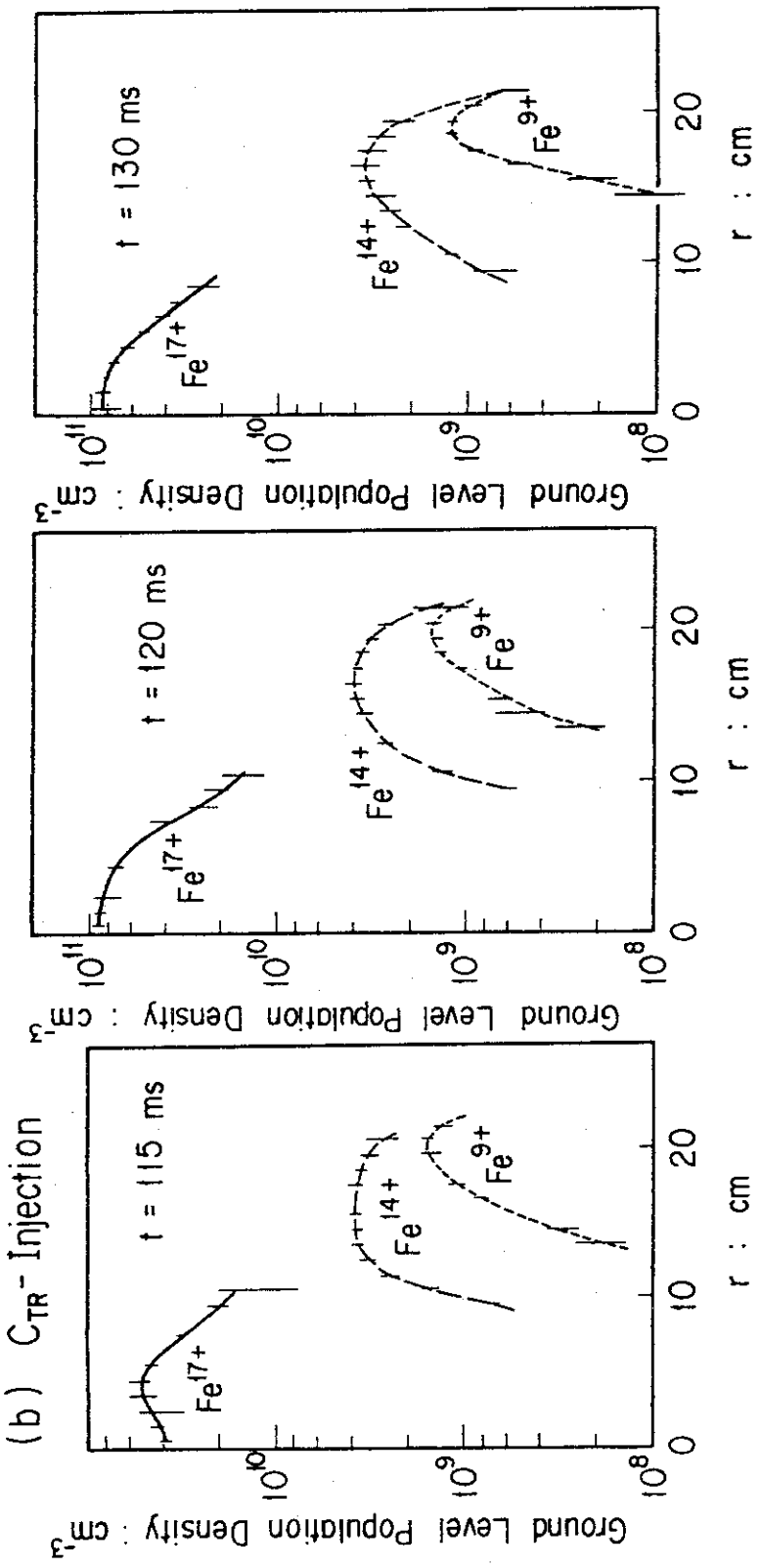
(b) C_{TR} - Injection
t = 115 ms
t = 120 ms
t = 130 ms
Fe^{17+}
Fe^{14+}
Fe^{9+}
Ground Level Population Density : cm^{-3}
r : cm
10^{11}
10^{10}
10^{9}
10^{8}
0
10
20

Fig. 7(b)

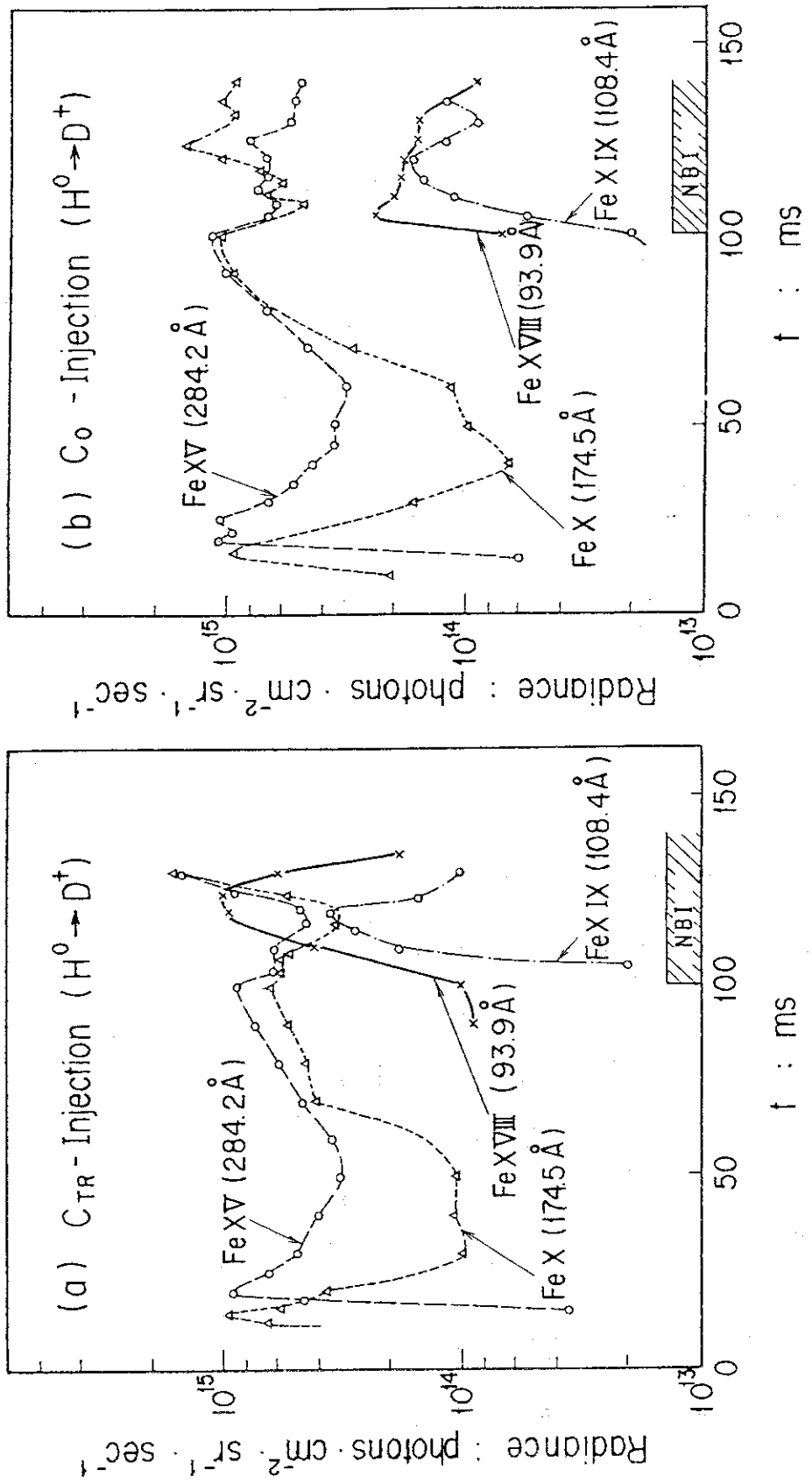

Fig. 8 Time-behaviours of the radiance of the FeX, FeXV, FeXVIII and FeXIX (λ=108.4 Å) in the counter-injected discharges without sawtooth oscillation (a), and in the co-injected discharges with sawtooth oscillation (b).

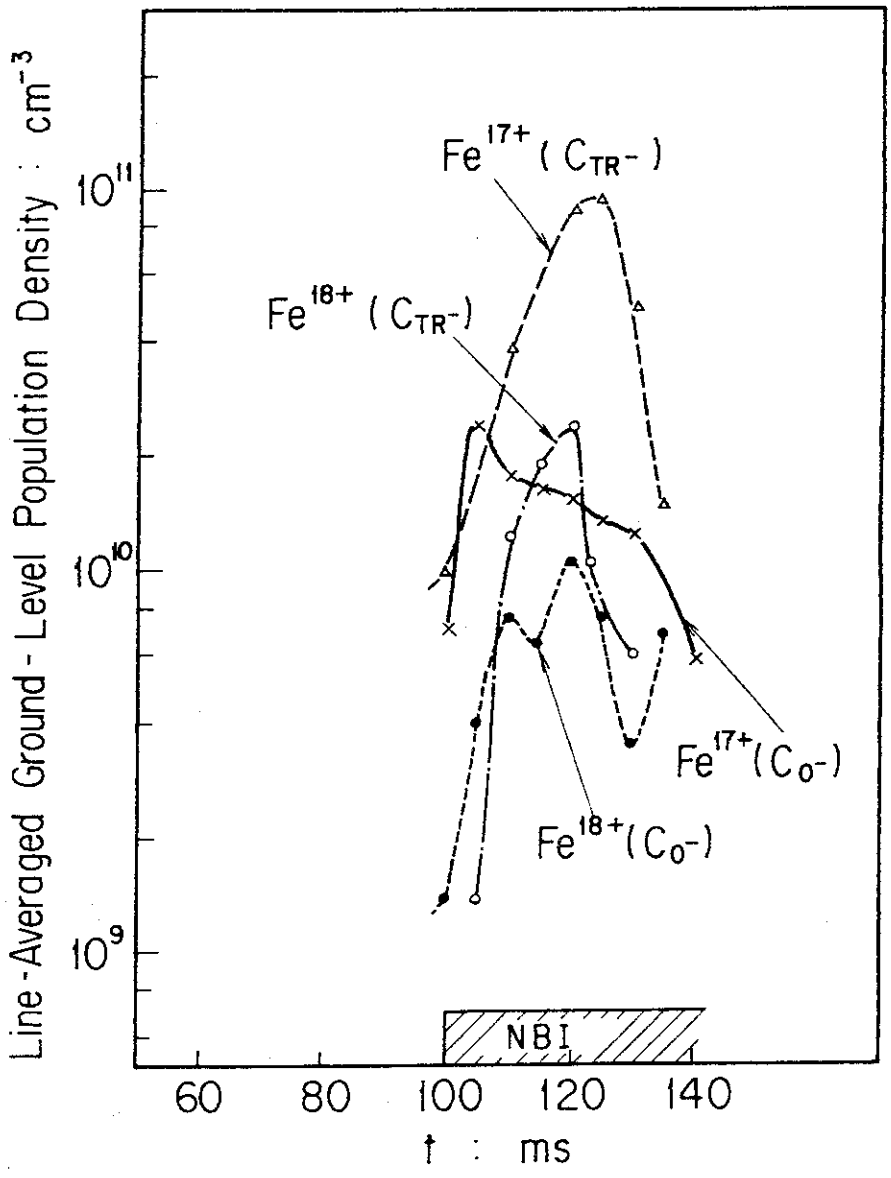

Fig. 9 Time-evolutions of the line-averaged population density of Fe^{17+} and Fe^{18+} ions in the ground state in counter-injection (C_{TR}-) and co-injection (C_0-).